Enhanced photocatalytic CO_2 reduction performance of Cu-Doped ZnO: synthesis, characterization, and mechanistic insights

Houdong Rao[1], Dongyang Zhang[2], Jingrui Li[3], Ling Zhang[4], Wei Cheng[5]
Luoyang Ship Material Research Institute, Luoyang, 471023, China
[1]Corresponding author
E-mail: [1]*838020036@qq.com*, [2]*zdy_dut@163.com*, [3]*wojiaojingrui@163.com*, [4]*zhangling918813@163.com*, [5]*chengwei@725.com.cn*

Received 24 December 2024; accepted 13 February 2025; published online 15 May 2025
DOI https://doi.org/10.21595/vp.2025.24745

72nd International Conference on Vibroengineering in Almaty, Kazakhstan, May 15-16, 2025

Abstract. In this study, we utilized in situ infrared spectroscopy to comprehensively analyze the behavior of copper-doped zinc oxide (Cu-ZnO) in photocatalytic CO_2 reduction reactions. By pyrolyzing copper-doped ZIF-8 precursors, we achieved a uniform distribution of copper within the zinc oxide matrix. Experiments conducted under simulated sunlight conditions demonstrated that Cu-ZnO exhibits enhanced activity and selectivity in the conversion of CO_2 to CO compared to undoped ZnO. The findings from in situ infrared spectroscopy indicate that copper doping significantly improves the material's ability to adsorb and activate CO_2, thereby enhancing its photocatalytic performance. This study has developed the application of in situ infrared spectroscopy in surface catalysis and provided a new direction for exploring the catalytic mechanism of photocatalytic CO_2 reduction.

Keywords: Cu, ZnO, In situ infrared, photocatalysis, CO2 reduction.

1. Introduction

Recently, in order to deal with a series of environmental and ecological problems caused by excessive CO_2 emissions, the scientific community has placed considerable emphasis on photocatalytic CO_2 conversion technology, recognizing it as a promising approach to transform CO_2 into valuable fuels or chemical feedstocks. [1] This technology holds the potential not only to mitigate the greenhouse effect but also to promote the sustainable utilization of energy through the conversion and storage of solar energy [2, 3]. Among various studies [4], the development of efficient, durable, and economically viable photocatalytic materials is seen as pivotal to advancing the practical application of photocatalytic CO_2 conversion technology. Specifically, the creation of high-efficiency photocatalytic materials is considered a critical step in overcoming existing technological bottlenecks [5, 6].

ZnO, due to its excellent light absorption properties and chemical stability, has been widely discussed as a photonic material. However, there remains room for enhancement in the photocatalytic efficiency of ZnO for practical applications [7]. Copper-based catalysts, known for their unique adsorption capabilities towards CO_2 and its reaction intermediates, have shown remarkable catalytic performance in CO_2 conversion [8-10]. The analytical methods include time-resolved Fourier transform infrared spectroscopy (FTIR) and time-resolved surface-enhanced Raman spectroscopy (SERS), which enable real-time monitoring of catalytic processes and capture of reaction intermediates, provide direct experimental evidence for elucidating reaction mechanisms [11, 12]. These techniques have played a significant role in understanding the chemical reaction mechanisms at the surface of copper-based catalysts, becoming key tools in the study of interfacial catalysis.

In this study, we employed high-temperature calcination to successfully synthesize polycrystalline ZnO and copper-doped polycrystalline ZnO (Cu-ZnO). Through experiments

simulating sunlight irradiation, we investigated the performance of polycrystalline ZnO in photocatalytic CO_2 reduction before and after copper doping. Our results show that, compared to undoped ZnO, the introduction of copper significantly enhances the CO_2 reduction rate and product selectivity of polycrystalline ZnO. Using in situ infrared spectroscopy, we explored the reaction mechanism of the catalyst and found that the addition of copper promotes the adsorption and activation of CO_2 by polycrystalline ZnO, facilitating the formation of key reaction intermediates such as *COOH, which in turn improves the catalytic efficiency of CO_2-to-CO conversion. This study provides important guidance for the design of more efficient photocatalytic systems and extends the application of infrared spectroscopy in exploring interfacial reaction mechanisms.

2. Experiment

2.1. Preparation of catalysts

2.1.1. Materials

Analysis of pure zinc acetate, methanol, dimethylimidazole, copper nitrate dihydrate, triethanolamine purchased from Balingwei Technology Co., LTD.

2.1.2. Sample preparation

Preparation of ZIF-8: In a standard synthesis procedure, zinc acetate (0.4 mmol) was dissolved in 80 mL of methanol to prepare solution A, while dimethylimidazolate (1.6 mmol) was dissolved in 100 mL of methanol to form solution B. Under continuous vigorous stirring, solution B was gradually added to solution A. The combined mixture was subsequently heated to 50 ℃ and maintained at this temperature with stirring for 2 hours. Upon completion of the reaction, the system was allowed to cool to ambient temperature naturally. The resulting product was isolated via centrifugation and underwent three wash cycles using deionized water and ethanol. Finally, the product was dried under vacuum at 60℃ overnight.

Preparation of Cu-ZIF-8: The synthesis procedure for Cu-ZIF-8 closely followed that of ZIF-8, with the only difference occurring in the preparation of solution A. For Cu-ZIF-8, solution A was prepared by dissolving 0.2 mmol of copper nitrate and 0.2 mmol of zinc acetate in 80 mL of methanol.

Preparation of ZnO and Cu-ZnO:To obtain the catalysts ZnO and Cu-ZnO, ZIF-8 and Cu-ZIF-8 were subjected to calcination at 450 °C for 2 hours in an air atmosphere.

2.2. Performance and characterization of samples

In evaluating the photocatalyst's performance in CO_2 conversion, the catalysts (5 mg) was added to a solution of 4 mL acetonitrile, 1 mL deionized water, and 1 mL triethanolamine. The setup was prepared by purging it with CO_2 for 30 minutes to create an reaction environment. A 300 W xenon lamp provided illumination during the experiment. Analysis of the gaseous products was conducted using a gas chromatograph (GC7920-TF2Z), which included thermal conductivity (TCD) and flame ionization (FID) detectors.

2.3. In-situ infrared spectroscopy characterization

For in-situ Fourier Transform Infrared (FT-IR) analysis, a Bruker Vertex 70 V spectrometer, fitted with a narrow-band HgCdTe detector and a transmission reaction cell from Harrick, was utilized. The system was connected to a molecular pump to achieve an ultra-high vacuum of approximately 10^{-7} mbar. A self-supported pellet, prepared by pressing 5 mg of the sample powder into a 7.0 mm diameter disk, was positioned within the transmission cell. During a standard in-

situ FT-IR measurement, the initial step involved evacuating the transmission cell to eliminate any adsorbed air. Next, CO_2 adsorption characteristics were examined using a gas stream containing 25 % CO_2. Following this, the cell was exposed to a CO_2 gas stream that had been saturated with water vapor to study both CO_2 and water adsorption simultaneously. Finally, the transmission cell was sealed to prepare for subsequent photocatalytic reactions

3. Results and discussion

3.1. Catalyst structure analysis

Initially, the structural morphologies of the synthesized ZnO and Cu-ZnO materials were investigated through transmission electron microscopy (TEM) analysis. As shown in Fig. 1(a) and c, the prepared ZnO and Cu-ZnO exhibit consistent morphologies, indicating that the introduction of Cu did not significantly alter the morphology of ZnO. To gain deeper insights into their lattice structures, High-Resolution Transmission Electron Microscopy (HRTEM) was utilized for detailed characterization. As depicted in Fig. 1(b) and (d), both ZnO and Cu-ZnO display a polycrystalline structure with intersecting lattice fringes. During the pyrolysis process, the topological structure of ZIF-8 collapses, and under the influence of oxygen, C, N, Zn, and Cu are oxidized. C and N transform into gases and disperse into the atmosphere, while Zn and Cu are oxidized to ZnO and CuO, respectively. However, due to the original random distribution of Cu within the topological structure, CuO is completely encapsulated by ZnO, resulting in no observable lattice fringes corresponding to CuO in the HRTEM images.

To confirm the presence of Cu, we conducted elemental distribution analysis on ZnO and Cu-ZnO. As shown in Fig. 2, for the prepared ZnO, the catalyst contains a small amount of residual C, with the mass ratio of Zn to O being approximately 4:1, and the molar ratio close to 1:1, thus confirming the formation of ZnO. For Cu-ZnO, the catalyst shows a minor presence of residual C and N, with the Cu to Zn ratio being about 1:10, indicating a limited Cu doping level, which further explains the absence of CuO lattice fringes in the HRTEM images. Additionally, the mass ratios of Cu, Zn, and O adhere to the stoichiometric ratios expected for ZnO and CuO. The aforementioned data confirm the successful synthesis of polycrystalline ZnO and Cu-ZnO.

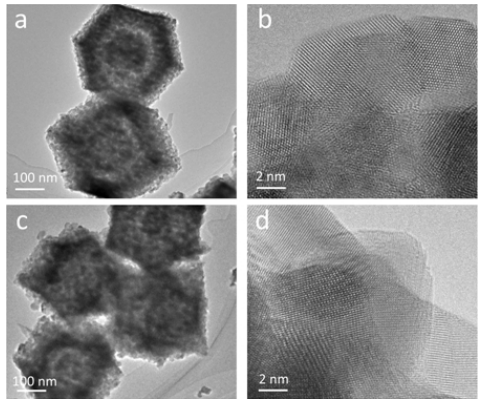

Fig. 1. TEM images: a), b) ZnO, c), d) Cu-ZnO

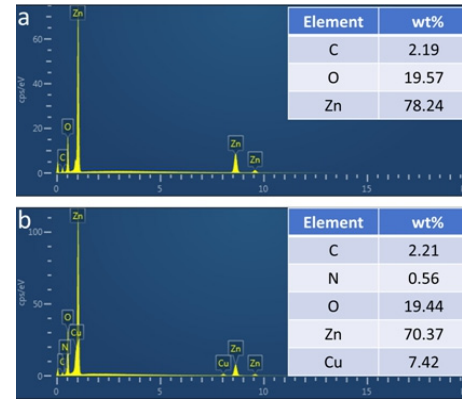

Fig. 2. EDS images: a) ZnO, b) Cu-ZnO

3.2. Evaluation of catalytic performance

As shown in Fig. 3(a) and (b), the primary products of photocatalytic CO_2 reduction for both ZnO and Cu-ZnO are carbon monoxide (CO) and hydrogen gas (H_2), where CO is derived from CO_2 reduction, and H_2 is mainly produced as a by-product through the photolysis of H_2O. Cu-ZnO achieved CO and H_2 production rates of 35 $\mu mol \cdot g^{-1} \cdot h^{-1}$ and 8 $\mu mol \cdot g^{-1} \cdot h^{-1}$, respectively, with a remarkable CO selectivity of up to 81 %. In stark contrast, undoped ZnO exhibited significantly

lower activity, with CO and H_2 production rates of 18 μmol·g^{-1}·h^{-1} and 22 μmol·g^{-1}·h^{-1}, respectively. Notably, the CO selectivity for undoped ZnO dropped to only 45 %, highlighting a substantial decrease in CO selectivity without Cu doping. This comparison clearly underscores the significant enhancement in both CO production rate and CO selectivity brought about by Cu doping, demonstrating its crucial role in improving the photocatalytic efficiency for CO2 reduction.

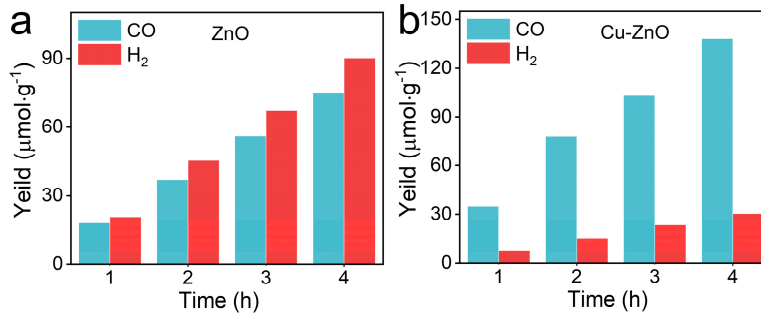

Fig. 3. Photocatalytic CO_2 reduction properties of ZnO, Cu-ZnO

3.3. Mechanistic insights

We first acquired the infrared data of ZnO and Cu-ZnO, as illustrated in Fig. 4. The prominent peak between 1200 and 1700 cm^{-1} and the peak above 3000 cm^{-1} are associated with O-H bonds. Some researchers suggest that the peak between 1200 and 1700 cm^{-1}were identified as C = C and C-H stretching vibrations in the carbon framework. However, when referencing the standard spectrum of graphene, the intensity of the C = C stretching vibration would not be this strong. The most plausible explanation is that the peak between 1200 and 1700 cm^{-1} includes O-H bending vibrations. Therefore, after the introduction of Cu, the number of surface hydroxyl groups on Cu-ZnO increases significantly. The increase in surface hydroxyl groups facilitates CO_2 adsorption, promoting the formation of surface $CO_3^{2-}$and HCO_3^-species, further promoting the performance of photocatalytic CO_2 reduction reactions.

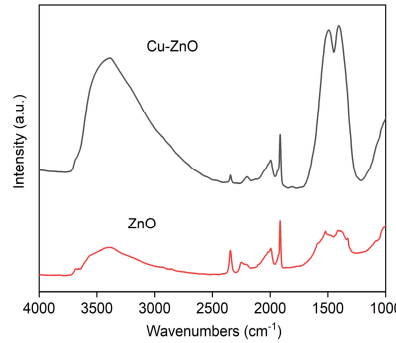

Fig. 4. Infrared spectrum of ZnO and Cu-ZnO

To gain a deeper understanding of the intrinsic reaction mechanisms responsible for the enhanced catalytic performance and selectivity of Cu-doped ZnO compared to pure ZnO in photocatalytic CO_2 reduction, this study utilized in-situ infrared spectroscopy to compare the CO_2 reduction processes of the two catalysts in detail. Fig. 5(a) illustrates the photocatalytic CO_2 reduction process over ZnO, where the negative peaks at 1476 and 1423 cm^{-1} are primarily attributed to the consumption of surface-adsorbed CO_2 species (CO_3^{2-} and HCO_3^-) and hydroxyl groups. Peaks corresponding to CO_2 reduction intermediates were not observed, likely due to

being overshadowed by the negative peaks, suggesting that the catalytic reaction is predominantly focused on hydrogen production with low selectivity for CO_2 conversion. Fig. 5(b) shows the photocatalytic CO_2 reduction process over Cu-ZnO, where peaks at 1574, 1450, 1375, and 1086 cm^{-1} are subject to the C-O stretching and O-H vibrations of the key intermediate *COOH in CO_2 reduction, indicating that the main reaction occurring on Cu-ZnO is the photocatalytic reduction of CO_2. The in-situ IR characterization suggests that the introduction of Cu significantly enhances the ability of ZnO to convert CO_2 into reactive intermediates.

Based on the aforementioned mechanistic discussion, it is evident that the introduction of Cu not only significantly enhances ZnO's ability to adsorb CO_2 but also boosts its capability to activate CO_2 into the key intermediate *COOH. Consequently, Cu-ZnO exhibits markedly improved performance in the photocatalytic reduction of CO_2 to CO compared to undoped ZnO.

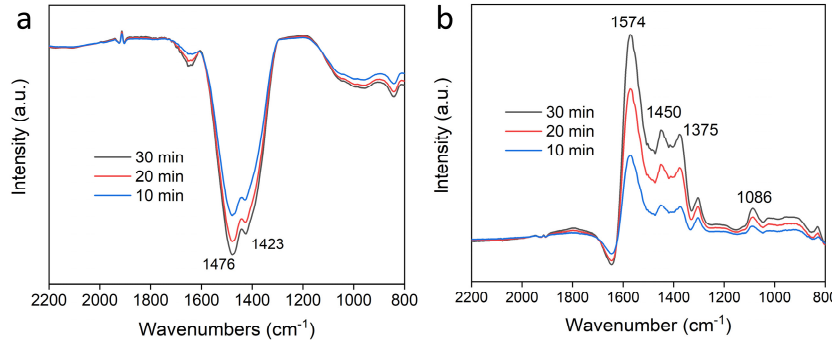

Fig. 5. In-situ infrared spectroscopy of a) ZnO and b) Cu-ZnO

4. Conclusions

This study successfully synthesized uniformly doped Cu-ZnO catalysts via high-temperature pyrolysis of Cu-doped ZIF-8, followed by detailed characterization and performance testing. Transmission Electron Microscopy (TEM) and High-Resolution Transmission Electron Microscopy (HRTEM) images indicated that Cu-ZnO retained a morphological structure similar to ZnO, with CuO being completely encapsulated by ZnO without noticeable changes in lattice fringes. Elemental Distribution Analysis (EDS) confirmed the doping of Cu, with a Cu/Zn ratio of approximately 1:10, indicating a low doping level of Cu. In terms of photocatalytic CO_2 reduction performance, Cu-ZnO demonstrated significantly superior performance compared to pure ZnO. The CO and H_2 production rates of Cu-ZnO reached 35 $\mu mol \cdot g^{-1} \cdot h^{-1}$ and 8 $\mu mol \cdot g^{-1} \cdot h^{-1}$, respectively, with a CO selectivity of up to 81%. In contrast, the CO and H_2 production rates of ZnO were 18 $\mu mol \cdot g^{-1} \cdot h^{-1}$ and 22 $\mu mol \cdot g^{-1} \cdot h^{-1}$, respectively, with a CO selectivity of only 45 %. These results indicate that the incorporation of Cu significantly enhances the CO_2 reduction efficiency and CO selectivity of ZnO. Additionally, in-situ infrared spectroscopy revealed an increased number of surface hydroxyl groups on Cu-ZnO, which is beneficial for CO_2 adsorption and accelerates the photocatalytic reduction rate of CO_2. In-situ infrared spectroscopy also showed that Cu-ZnO produces more key intermediates (*COOH) during CO_2 reduction, further demonstrating that the introduction of Cu enhances the CO_2 conversion capability of the ZnO catalyst. The novelty of this work lies in its pioneering use of in situ infrared spectroscopy to elucidate the catalytic mechanisms at play, offering unprecedented insights into the surface chemistry of Cu-ZnO. This study not only advances the application of in situ spectroscopy in surface catalysis but also sets a new direction for exploring the mechanistic details of photocatalytic CO_2 reduction. By highlighting these innovative aspects, we aim to attract attention and citations from the international engineering community, contributing to the development of more efficient and sustainable CO_2 conversion technologies.

As a common non-precious metal catalyst system, Cu-ZnO catalysts offer advantages such as

ISSN PRINT 2345-0533, ISSN ONLINE 2538-8479

simple synthesis, ease of scalable production, and low cost, which can significantly advance the photocatalytic resource conversion of CO_2. This technology can serve as a means for CO_2 emission reduction in industrial exhaust gas treatment systems or be integrated into solar fuel production equipment to generate renewable fuels. These applications have the potential to contribute substantially to addressing environmental challenges and promoting sustainable energy development.

Acknowledgements

The authors have not disclosed any funding.

Data availability

The datasets generated during and/or analyzed during the current study are available from the corresponding author on reasonable request.

Conflict of interest

The authors declare that they have no conflict of interest.

References

[1] K. Kosugi, C. Akatsuka, H. Iwami, M. Kondo, and S. Masaoka, "Iron-complex-based supramolecular framework catalyst for visible-light-driven CO2 reduction," *Journal of the American Chemical Society*, Vol. 145, No. 19, pp. 10451–10457, May 2023, https://doi.org/10.1021/jacs.3c00783

[2] H. Huang et al., "Noble-metal-free high-entropy alloy nanoparticles for efficient solar-driven photocatalytic CO2 reduction," *Advanced Materials*, Vol. 36, No. 26, Apr. 2024, https://doi.org/10.1002/adma.202313209

[3] Z. Xie et al., "Well-defined diatomic catalysis for photosynthesis of C2H4 from CO2," *Nature Communications*, Vol. 15, No. 1, p. 2422, Mar. 2024, https://doi.org/10.1038/s41467-024-46745-3

[4] W. Zhang, Y. Huang, J. Shao, and H. Wu, "Research progress of semiconductor nanophotocatalyst," (in Chenese), *Development and Application of Materials*, Vol. 27, No. 3, 2012, https://doi.org/10.19515/j.cnki.1003-1545.2012.03.021

[5] X. Wang et al., "Gold-in-copper at low *CO coverage enables efficient electromethanation of CO2," *Nature Communications*, Vol. 12, No. 1, p. 3387, Jun. 2021, https://doi.org/10.1038/s41467-021-23699-4

[6] J. Zhao et al., "Modulation of *CHxO adsorption to facilitate electrocatalytic reduction of CO2 to CH4 over cu-based catalysts," *Journal of the American Chemical Society*, Vol. 145, No. 12, pp. 6622–6627, Mar. 2023, https://doi.org/10.1021/jacs.2c12006

[7] X. Li et al., "Selective visible-light-driven photocatalytic CO2 reduction to CH4 mediated by atomically thin CuIn5S8 layers," *Nature Energy*, Vol. 4, No. 8, pp. 690–699, Jul. 2019, https://doi.org/10.1038/s41560-019-0431-1

[8] D. He, T. Li, X. Dai, S. Liu, X. Cui, and F. Shi, "Construction of highly active and selective molecular imprinting catalyst for hydrogenation," *Journal of the American Chemical Society*, Vol. 145, No. 38, pp. 20813–20824, Sep. 2023, https://doi.org/10.1021/jacs.3c04576

[9] J. B. Ernst et al., "Molecular adsorbates switch on heterogeneous catalysis: induction of reactivity by n-heterocyclic carbenes," *Journal of the American Chemical Society*, Vol. 139, No. 27, pp. 9144–9147, Jul. 2017, https://doi.org/10.1021/jacs.7b05112

[10] D. Wu et al., "Surface molecular imprinting over supported metal catalysts for size-dependent selective hydrogenation reactions," *Nature Catalysis*, Vol. 4, No. 7, pp. 595–606, Jul. 2021, https://doi.org/10.1038/s41929-021-00649-3

[11] L. Chen, X. Wang, W. Lu, X. Wu, and J. Li, "Molecular imprinting: perspectives and applications," *Chemical Society Reviews*, Vol. 45, No. 8, pp. 2137–2211, Jan. 2016, https://doi.org/10.1039/c6cs00061d

[12] C. P. Canlas et al., "Shape-selective sieving layers on an oxide catalyst surface," *Nature Chemistry*, Vol. 4, No. 12, pp. 1030–1036, Oct. 2012, https://doi.org/10.1038/nchem.1477